# Magnetic helicity: applications in solar physics

A. Nindos

Physics Department, University of Ioannina, Greece

# Outline

- Basic definitions and properties
- Useful decompositions
- Computation methods
- Helicity and large eruptive events
- Helicity and jets
- Conclusions

# Magnetic helicity

Magnetic helicity is a conserved quantity that describes the field's topological complexity by measuring the twist, writhe, and linkage of the field lines

$$H = \int_V \mathbf{A} \cdot \mathbf{B} \, dV$$

where $\boldsymbol{B}$ is the magnetic field and $\boldsymbol{A}$ is the magnetic vector potential

- Units: magnetic flux squared (SI -> $Wb^2$, cgs -> $Mx^2$)
- Signed scalar quantity: right-handed (+) or left-handed (-)

# Why is helicity a measure of magnetic linkage (case of two unknotted flux tubes with no internal twist)

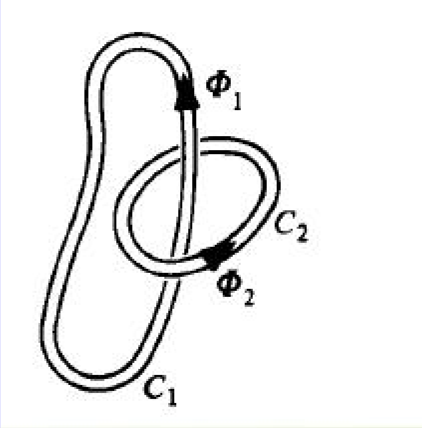


$H = 2\Phi_1 \Phi_2$

- Consider two thin linked magnetic flux tubes with cross sectional area vectors $d\mathbf{S}_1$ and $d\mathbf{S}_2$. Let $\Phi_1 = \int \mathbf{B}_1 \cdot d\mathbf{S}_1$ be the magnetic flux in tube 1, where $\mathbf{B}_1$ is the magnetic field. Similarly, for flux tube 2 we have $\Phi_2 = \int \mathbf{B}_2 \cdot d\mathbf{S}_2$ where $\mathbf{B}_2$ is the magnetic field.

- We can split the magnetic helicity into contributions from the two flux tube volumes to obtain

$$\int \mathbf{A} \cdot \mathbf{B} dV = \iint \mathbf{A}_1 \cdot \mathbf{B}_1 dl_1 dS_1 + \iint \mathbf{A}_2 \cdot \mathbf{B}_2 dl_2 dS_2$$

$$\int \mathbf{A} \cdot \mathbf{B} dV = \int A_1 dl_1 \int B_1 dS_1 + \int A_2 dl_2 \int B_2 dS_2 = \Phi_2 \Phi_1 + \Phi_1 \Phi_2 = 2\Phi_1 \Phi_2$$

where we have used Gauss' theorem to replace $\int A_1 dl_1 = \Phi_2$, the magnetic flux of tube 2 that is linked through tube 1 and similarly $\int A_2 dl_1 = \Phi_1$

# Gauge dependence

For a vector potential A, the addition of the gradient of a scalar function, i.e. the transformation $A \rightarrow A+\nabla\psi$, does not change the resulting B. This property of the definition of B is called gauge-invariance

Due to this freedom in the gauge, *H* is not uniquely defined, since

$$\mathscr{H}(\mathbf{A}+\nabla\psi) = \mathscr{H}(\mathbf{A}) + \int_{\partial\mathcal{V}} (\psi\mathbf{B})\cdot d\mathbf{S} - \int_{\mathcal{V}} \psi\,(\nabla\cdot\mathbf{B})\,d\mathcal{V}$$

Hence, *H* is gauge invariant only if two conditions are met:

- B must be solenoidal, as implied by its definition as curl of A
- The volume's bounding surface ∂V must be a flux surface of B, i.e. $(B \cdot \hat{n})|_{\partial V} = 0$

-- The solenoidal requirement is satisfied by virtue of Maxwell's equations
-- ∂V is a flux surface if no magnetic field line is threading the boundary (as for a closed field)
This latter requirement is rarely satisfied in natural systems, which often contain open magnetic fields, and makes Eq. $H=\int A\cdot B\,dV$ of limited interest for practical use

# Relative magnetic helicity

For a domain like the corona with boundaries that are not flux surfaces we introduce the relative magnetic helicity of $B$ with respect to the helicity of a reference field $B_p$ having the same distribution of $B_n$ on the surface $S$ surrounding $V$ (Berger & Field 1984 Finn & Antonsen 1985)

$$H_r = \int_V (\mathbf{A} + \mathbf{A}_p) \cdot (\mathbf{B} - \mathbf{B}_p)\, dV$$

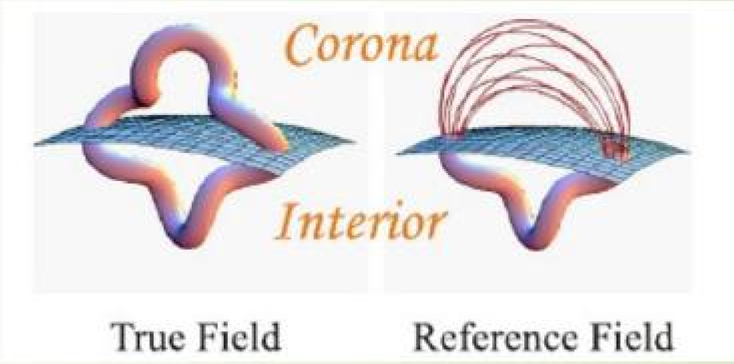


where $\boldsymbol{B}_p = \text{curl}\, \boldsymbol{A}_p$ is a field that is potential inside $V$. It is also the same as $\boldsymbol{B}$ outside $V$ and satisfies $\boldsymbol{A} \times \boldsymbol{n}|_S = \boldsymbol{A}_p \times \boldsymbol{n}|_S$.

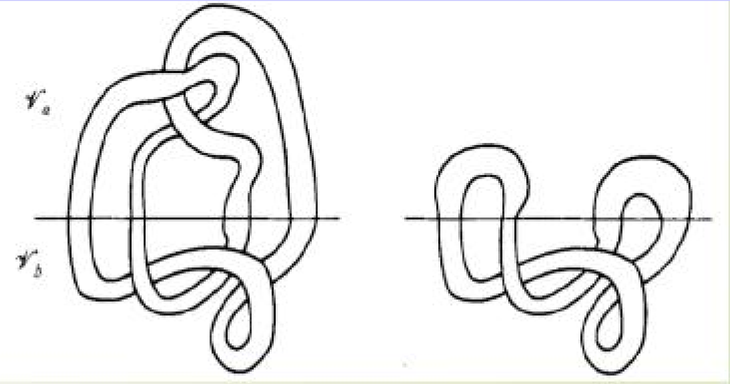

- A potential field is a convenient choice of $\boldsymbol{B}_p$ which satisfies the condition curl $\boldsymbol{B}_p = 0$ and $\boldsymbol{B} \cdot \boldsymbol{n}|_S = \boldsymbol{B}_p \cdot \boldsymbol{n}|_S$
- It is gauge invariant
- It has all the physical properties of magnetic helicity

# Self & mutual helicity

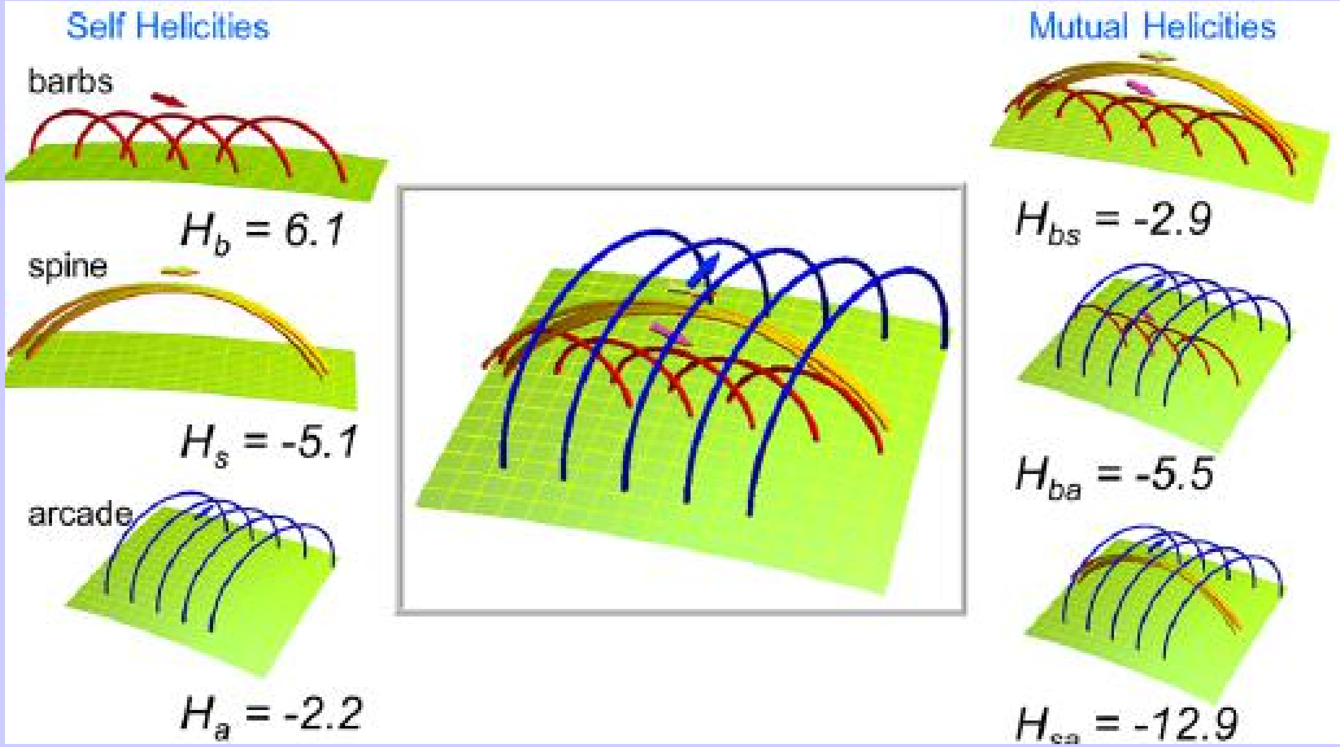


Cartoon model of a prominence field. The magnetic flux has been divided into distinct regions corresponding to arcade fields on top, the axis field going all the way along the prominence, and barb fields below. The self helicities of each region are shown on the left, while their mutual helicities are shown on the right (Image credit: M. Berger)

- Suppose we divide the magnetic field in a volume V into two or more distinct components
- What happens when we restrict the sum to pairs where both lines stay/belong to one component?
- --> we obtain the self-helicity of the component. If we look at all pairs where one line is in one component and a second line is in another component, then we obtain the mutual helicity between the two components.
- See this cartoon: Each component can have its own self-helicity due to its internal twist and shear. In addition, two different components will share a mutual helicity due to their interlinking

# Helicity of an isolated flux tube: twist and writhe

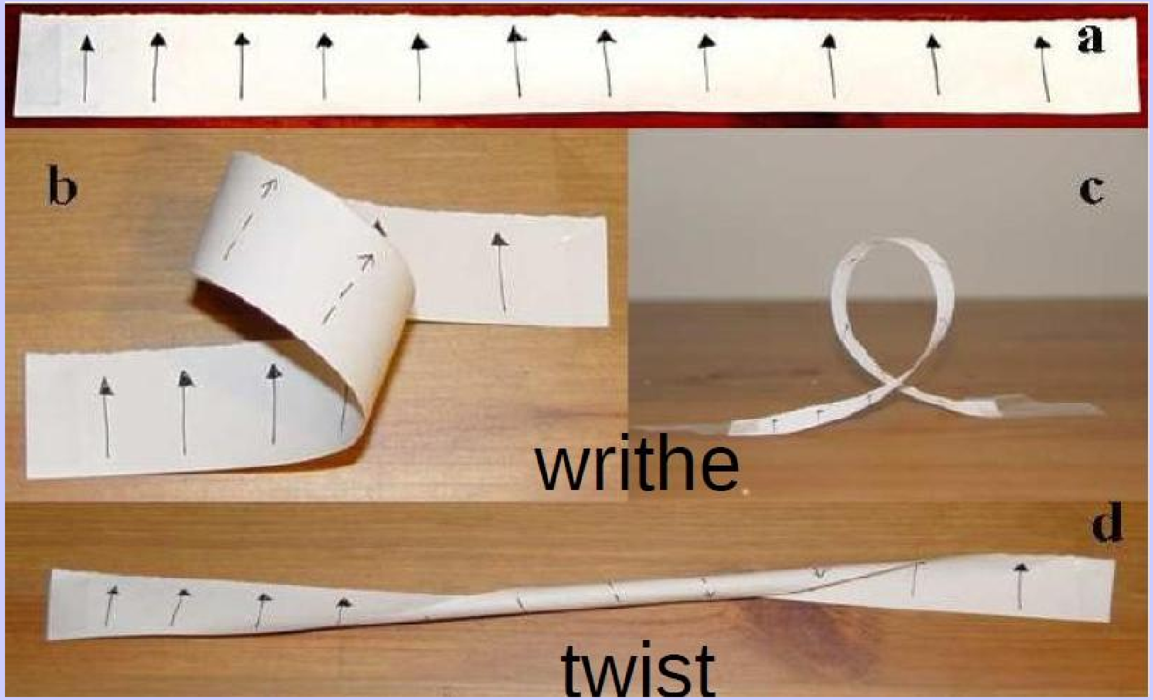


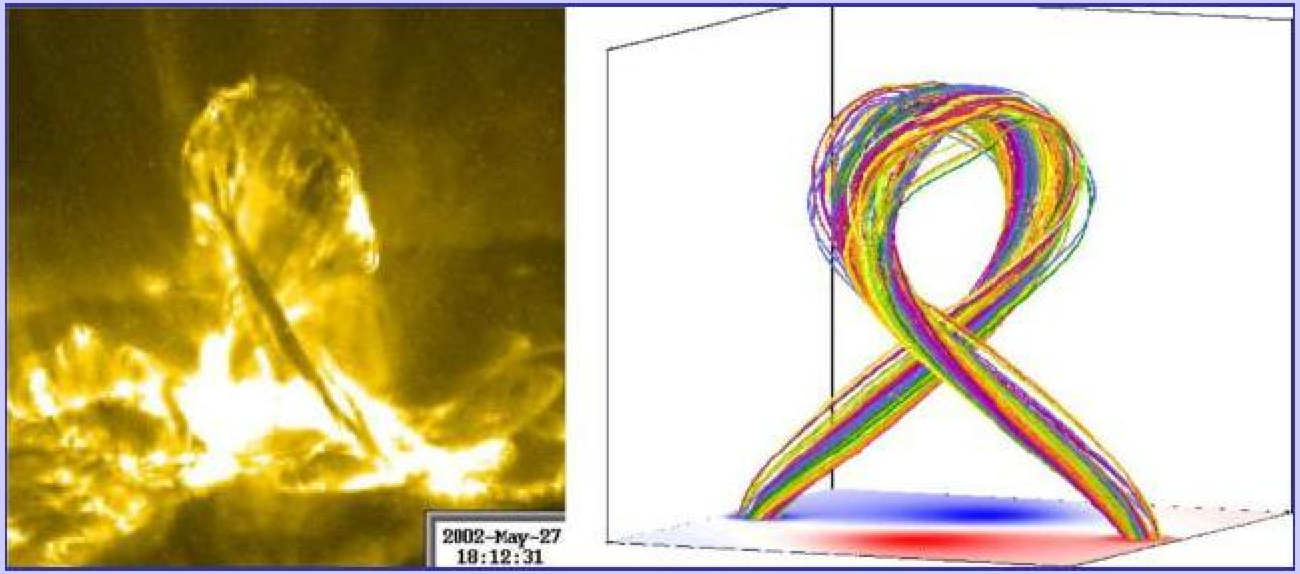


- Helicity of isolated magnetic flux tube: sum of twist and writhe: $H^{rel}_m = (Tw + Wr)\ \Phi^2$.

- Twist and writhe often confused:
  - -- Twist = winding of field lines about flux tube axis
  - -- Writhe = quantifies the helical deformation of the axis itself
- Kink instability: twist ↓ and writhe ↑ (sum is constant)

# Twist and writhe: a solar example

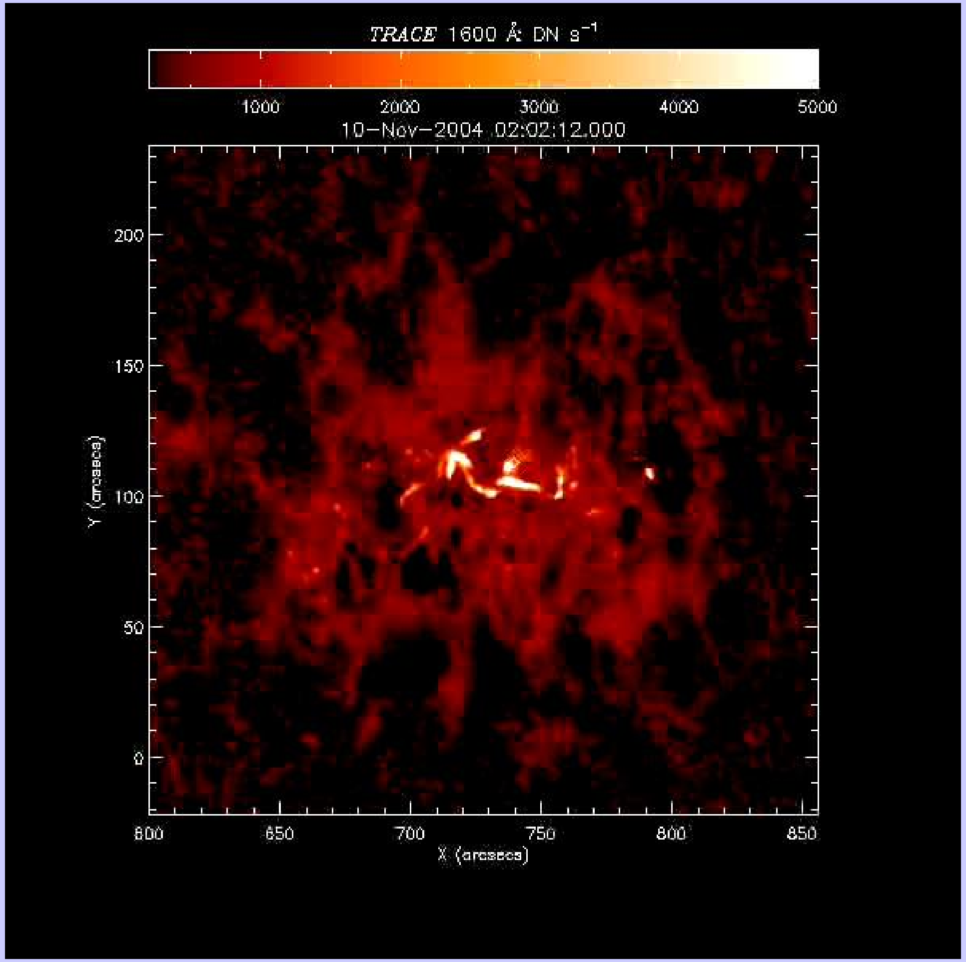


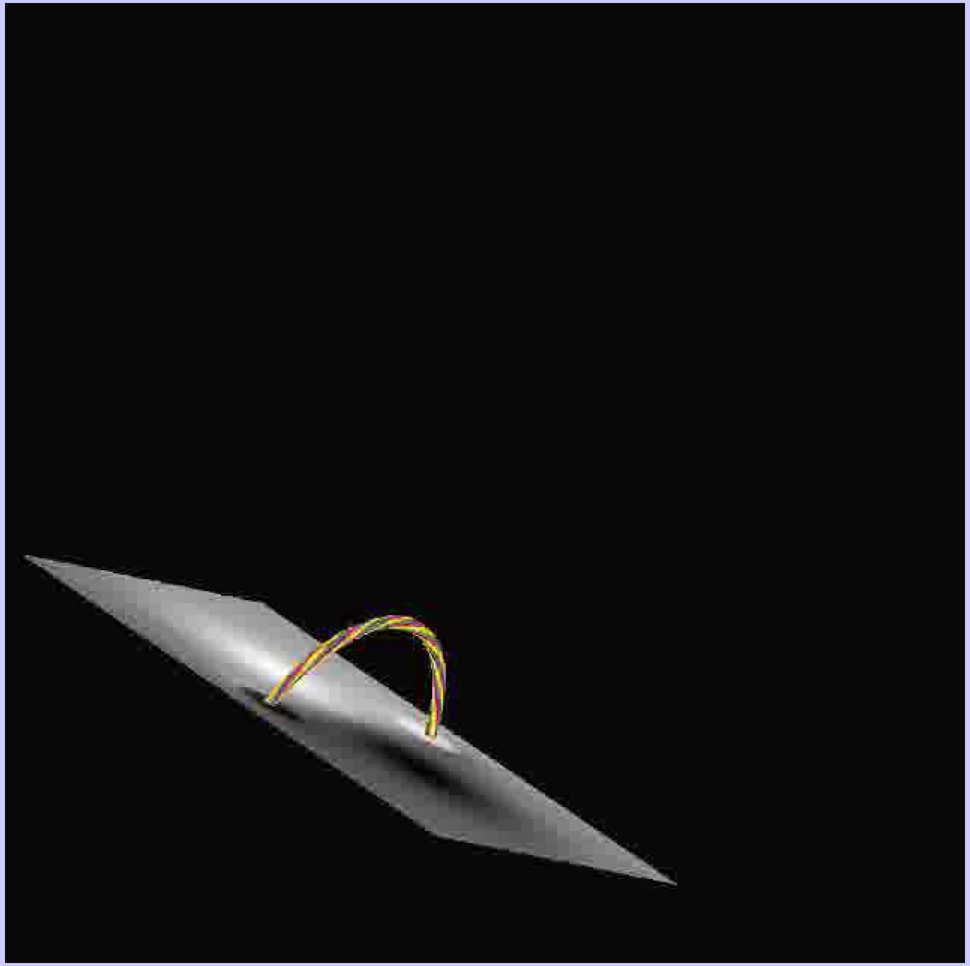

From Williams et al. (2005)

# Another useful decomposition

- Helicity can be split into two gauge-invariant components following the decomposition of the magnetic field to a potential component and a current-carrying component

$$B = B_p + B_j$$

$$H_r = H_j + H_{pj}$$

$$H_j = \int_V (\mathbf{A} - \mathbf{A}_\mathrm{p}) \cdot (\mathbf{B} - \mathbf{B}_\mathrm{p}) \, \mathrm{d}V$$

$$H_{pj} = 2 \int_V \mathbf{A}_\mathrm{p} \cdot (\mathbf{B} - \mathbf{B}_\mathrm{p}) \, \mathrm{d}V$$

- The ratio of the magnetic helicity of the current-carrying field to the total magnetic helicity is named **helicity index** by some authors (e.g. Pariat et al. 20xx)

# Conservation of helicity

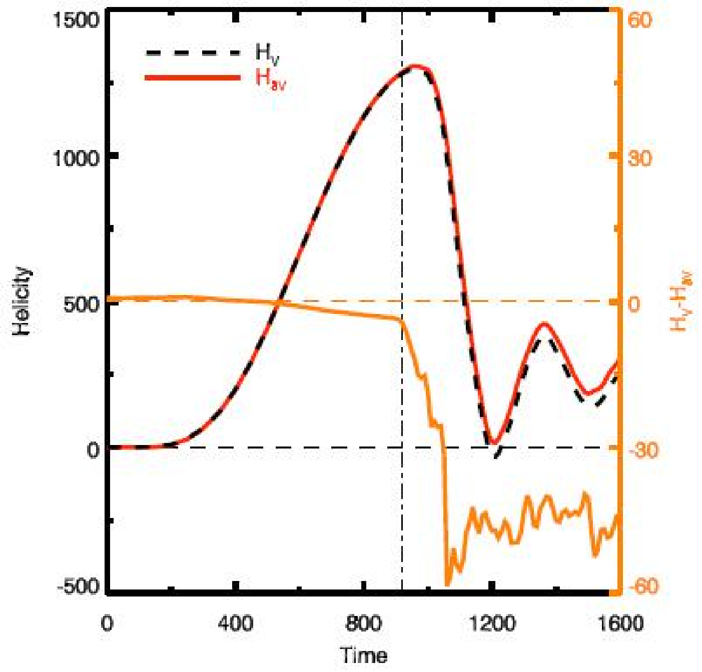


Comparison of the evolution of helicity obtained by volume integration (black dashed line) with the time integration of the helicity flux through the whole surface of the domain (red line). Their difference is plotted in orange on a different range of amplitude (cf. right axis) (From Pariat et al. 2015)

- For a perfectly conducting plasma (the ideal MHD limit), the total helicity remains invariant during the evolution of any closed flux system and the minimum energy state of this system corresponds to a linear force-free magnetic field configuration satisfying the equation $\nabla \times B = \alpha B$ (Woltjer 1958)

- *H* can be regarded as an almost conserved quantity even in resistive MHD when the magnetic Reynolds number is large. The dissipation rate of magnetic helicity is negligible in all non-ideal processes, including reconnection (Taylor 1974; Pariat et al. 2015)

- Unlike energy helicity cascades inversely from small scales to large scales and also dissipates slower than energy in non-ideal MHD

# Helicity computation methods

**Table 1** Synoptic view of helicity computation methods, their properties and formulation, as described in Sect. 1.2. The subset of methods actually tested in this paper is listed in Table 2

| *Finite volume (FV)* | *Helicity-flux integration (FI)* |
|---|---|
| $\mathcal{H}_\mathcal{V} = \int_\mathcal{V} (\mathbf{A} + \mathbf{A}_\mathrm{p}) \cdot (\mathbf{B} - \mathbf{B}_\mathrm{p})\, \mathrm{d}\mathcal{V}$ <br> see Eq. (3) | $\frac{\mathrm{d}\mathcal{H}_\mathcal{V}}{\mathrm{d}t} = 2 \int_{\partial\mathcal{V}} [(\mathbf{A}_\mathrm{p} \cdot \mathbf{B}) v_n - (\mathbf{A}_\mathrm{p} \cdot \mathbf{v}_\mathrm{t}) B_n]\, \mathrm{d}S$ |
| – Requires $\mathbf{B}$ in $\mathcal{V}$ *e.g.*, from MHD simulations or NLFFF <br> – Compute $\mathcal{H}_\mathcal{V}$ at one time <br> – May employ different gauges (see Table 2) | – Requires time evolution of vector field on $\partial\mathcal{V}$ <br> – Requires knowledge or model of flows on $\partial\mathcal{V}$ <br> – Valid for a specific set of gauge and assumptions, see Pariat et al. (2017) |

| *Discrete flux-tubes (DT)* <br> $\mathcal{H} \simeq \sum_{i=1}^M \mathcal{T}_i \Phi_i^2 + \sum_{i=1}^M \sum_{j=1, j\neq i}^M \mathcal{L}_{i,j} \Phi_i \Phi_j$, <br> see Eq. (31) | |
|---|---|
| *Twist-number (TN)* <br> $\mathcal{H} \simeq \mathcal{T} \Phi^2$ <br> see Eq. (32) | *Connectivity-based (CB)* <br> $\mathcal{H} = A \sum_{i=1}^M \alpha_i \Phi_i^{2\delta} + \sum_{l,m=1}^M \mathcal{L}_{lm} \Phi_l \Phi_m$ <br> see Eq. (35) |
| – Estimation of the twist contribution to $\mathcal{H}$ <br> – Requires $\mathbf{B}$ in $\mathcal{V}$ <br> – Requires a flux-rope-like structure for computing the twist $\mathcal{T}$ | – Requires the vector field on photosphere at one time <br> – Models the corona connectivity as a collection of $M$ force-free flux tubes <br> – Minimal connection length principle |

From Valori et al. (2016)

# Connectivity-based method

Calculate the relative magnetic helicity and free magnetic energy assumimg that the coronal field can be represented by a collection of slender discrete flux tubes with different $\alpha$-parameter (NLFF) which are used for the construction of a flux-connectivity matrix on the photosphere (Georgoulis et al. 2012)

<u>Steps</u>:

1. Partition vector magnetogram into magnetic flux concentrations (MCT model, Barnes et al. 2005)
2. Create connectivity matrix with flux committed to opposite polarity partitions (simulated annealing method, Press et al. 1992)
   Criteria: (i) to connect regions of opposite polarity with the shortest possible distance, and (ii) these regions must have equal absolute-value magnetic fluxes
3. Each connection = flux tube with known flux, $\alpha$-parameter, position

self terms — mutual terms

$$H_m = H_{m_{self}} + H_{m_{mutual}} = 8\pi d^2 A \sum_{l=1}^{N} \alpha_l \Phi_l^{2\lambda} + \sum_{l=1}^{N} \sum_{m=1, l\neq m}^{N} \mathcal{L}_{lm}^{arch} \Phi_l \Phi_m$$

self terms — mutual terms

$$E_f = E_{f_{self}} + E_{f_{mutual}} = A d^2 \sum_{l=1}^{N} \alpha_l^2 \Phi_l^{2\lambda} + \frac{1}{8\pi} \sum_{l=1}^{N} \sum_{m=1, l\neq m}^{N} \alpha_l \mathcal{L}_{lm}^{arch} \Phi_l \Phi_m$$

- $l$, $m$: different flux tubes with known flux ($\Phi$) and $\alpha$ parameter
- $L_{lm}^{arch}$: mutual helicity parameter between two flux tubes $l$ and $m$
- $d$: pixel size
- $A$, $\lambda$: scaling constants (known)

# Helicity flux integration method: calculate helicity injection rates

$\Delta H_{\text{inj}}$, $\Delta E_{\text{inj}}$: the total accumulated helicity and energy injected into the corona between two given times $T_1$, $T_2$ - Helicity flux integration method

Compute the rates of magnetic helicity and magnetic energy injection into the corona (Berger 1984, 1999, Kusano et al. 2002):

$$\left.\frac{dH}{dt}\right|_S = 2\int_S (\boldsymbol{A_P}\cdot\boldsymbol{B_t})\,V_{\perp n}\,dS - 2\int_S (\boldsymbol{A}_{\mathrm{P}}\cdot\boldsymbol{V}_{\perp t})\mathrm{B}_n\,dS$$

emergence term shear term

$$\left.\frac{d\mathrm{E}}{dt}\right|_S = \frac{1}{4\pi}\int_S \mathrm{B}_t^2 V_{\perp n}\,dS - \frac{1}{4\pi}\int_S (\boldsymbol{B}_t\cdot\boldsymbol{V}_{\perp t})\,\mathrm{B}_n\,dS$$

- $\boldsymbol{A}_{\mathrm{p}}$: vector potential of the potential field $\boldsymbol{B}_{\mathrm{p}}$
- $\boldsymbol{B}_{\mathrm{t}}$, $\boldsymbol{B}_{\mathrm{n}}$: tangential and normal components of the magnetic field in the photosphere
- $\boldsymbol{V}_{\mathrm{perp,t}}$, $\boldsymbol{V}_{\mathrm{perp,n}}$: tangential and normal components of the velocity $\boldsymbol{V}_{\mathrm{perp}}$ which is perpendicular to the field lines

$$\Delta H_{inj} = \int_{T_1}^{T_2}\frac{dH}{dt}\,, \quad \Delta E_{inj} = \int_{T_1}^{T_2}\frac{dE}{dt}$$

# Comparison of different methods using the same observations

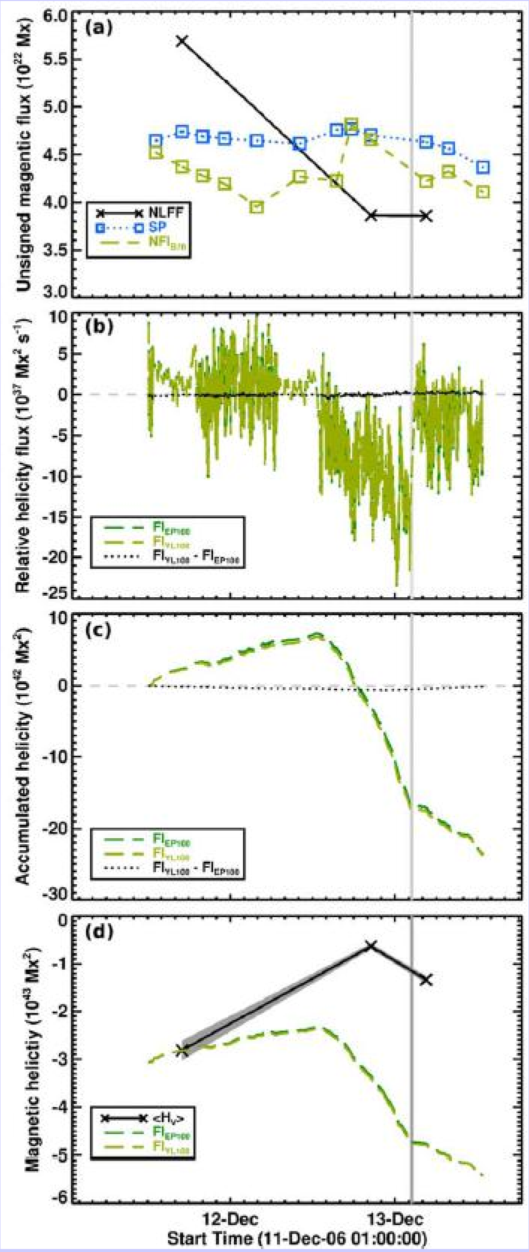


Unsigned flux

dH/dt from FI method

ΔH resulting from dH/dt

H from FV method (black)
ΔH resulting from dH/dt (green)

Thalmann et al. (2021)

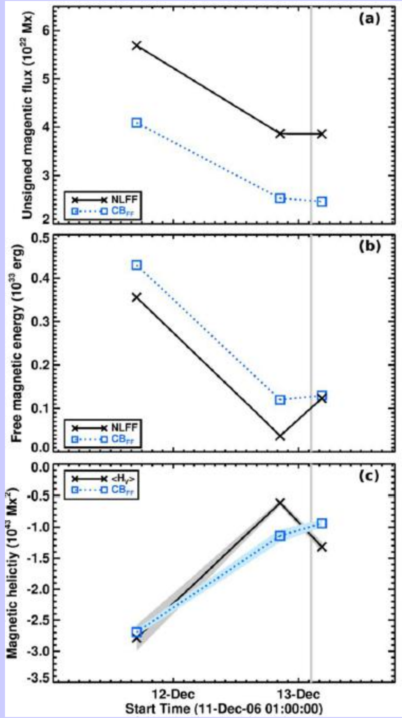


Unsigned flux

Free magnetic energy from NLFF (black)
Free magnetic energy from CB method (blue)

Helicity from FV method (black)
Helicity from CB method (blue)

- Strong agreement among the finite-volume methods
- Moderate agreement between the connectivity-based and finite-volume methods
- Excellent agreement between the flux-integration methods
- Overall agreement between finite-volume- and flux-integration-based estimates regarding the predominant sign and magnitude of the helicity

# A “unified approach” for the initiation of flares-CMEs

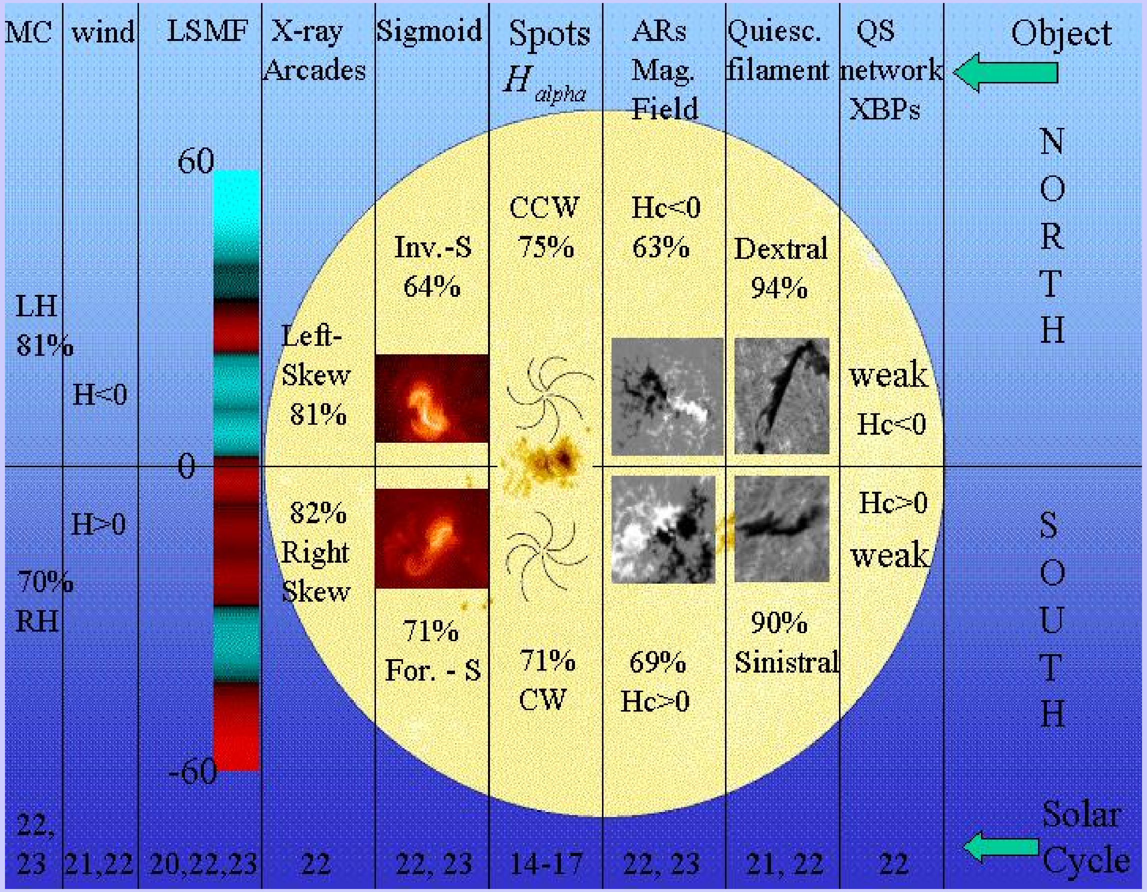


- The role of free magnetic energy in the initiation of solar eruptions is well established (e.g. Neukirch 2005)
- Role of magnetic helicity is debated **BUT**

  **Magnetic fields emerge with a preferred sign in each hemisphere**

**So, Magnetic Helicity is accumulating in the corona**

(Image credit: A. Pevtsov)

# CMEs as agents to releave the Sun from excess helicity

On the global scale mutual cancellation of *H* of opposite signs can’t relieve the Sun from excess accumulated *H*.

CMEs as expulsions of twisted m.f. consist the main process through which accumulated *H* is removed from the corona (Low, 1994; 1996)

# Some old first results supporting the above narrative

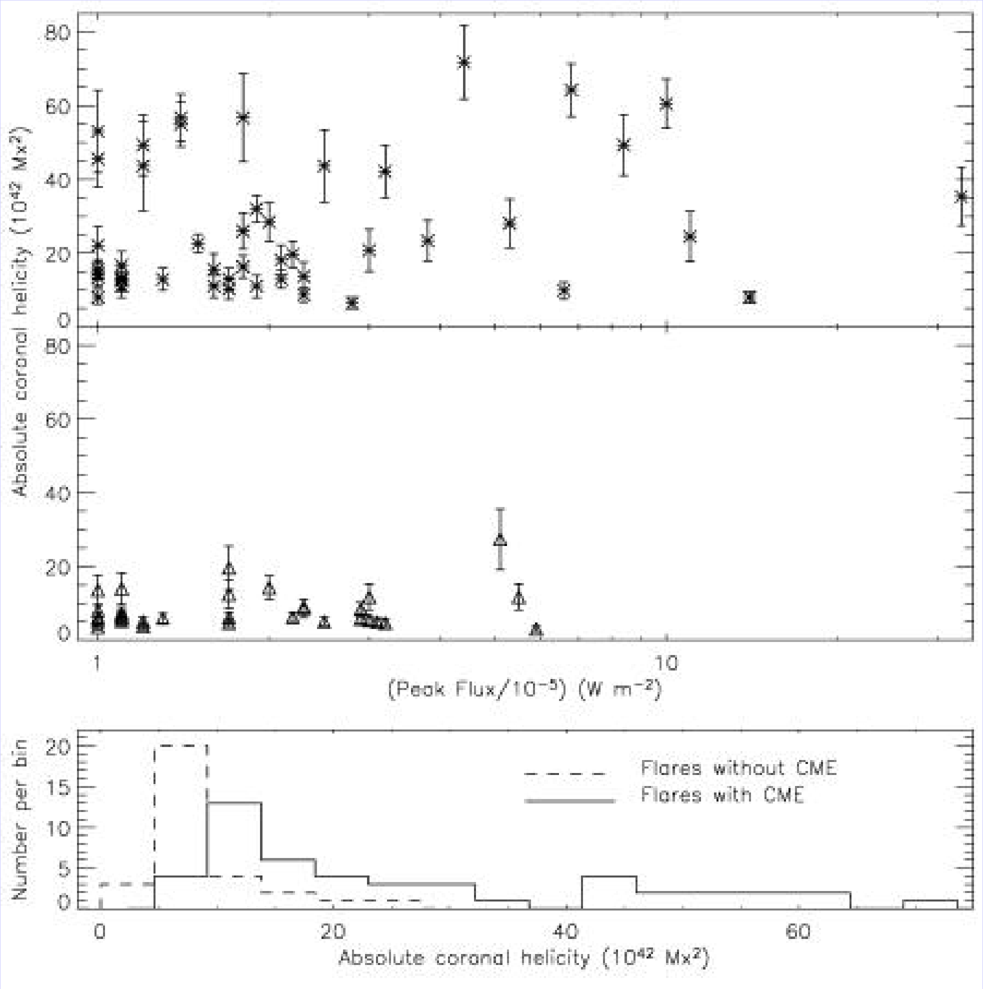


Scatter plot of the preflare absolute values of coronal helicity, $H_{cor}$, (from alpha-best) as a function of the flare's peak X-ray flux for ARs producing CME-associated M/X-class flares. Middle: Same as the top panel, but for the ARs producing M/X-class flares that do not have associated CMEs. Bottom: Histograms of the values of $H_{cor}$ appearing in the top and middle panels. The solid line is the histogram of $H_{cor}$ of the ARs that give CME-associated flares, and the dashed line is the histogram of $H_{cor}$ of the ARs that produce flares that do not have CMEs (Nindos & Andrews 2004)

In a statistical sense, the coronal helicity resulting from the absolute values of the linear force-free field parameter is higher in ARs that produce major eruptive flares than in those that produce major confined flares

# Helicity and free energy thresholds for the production of eruptive events

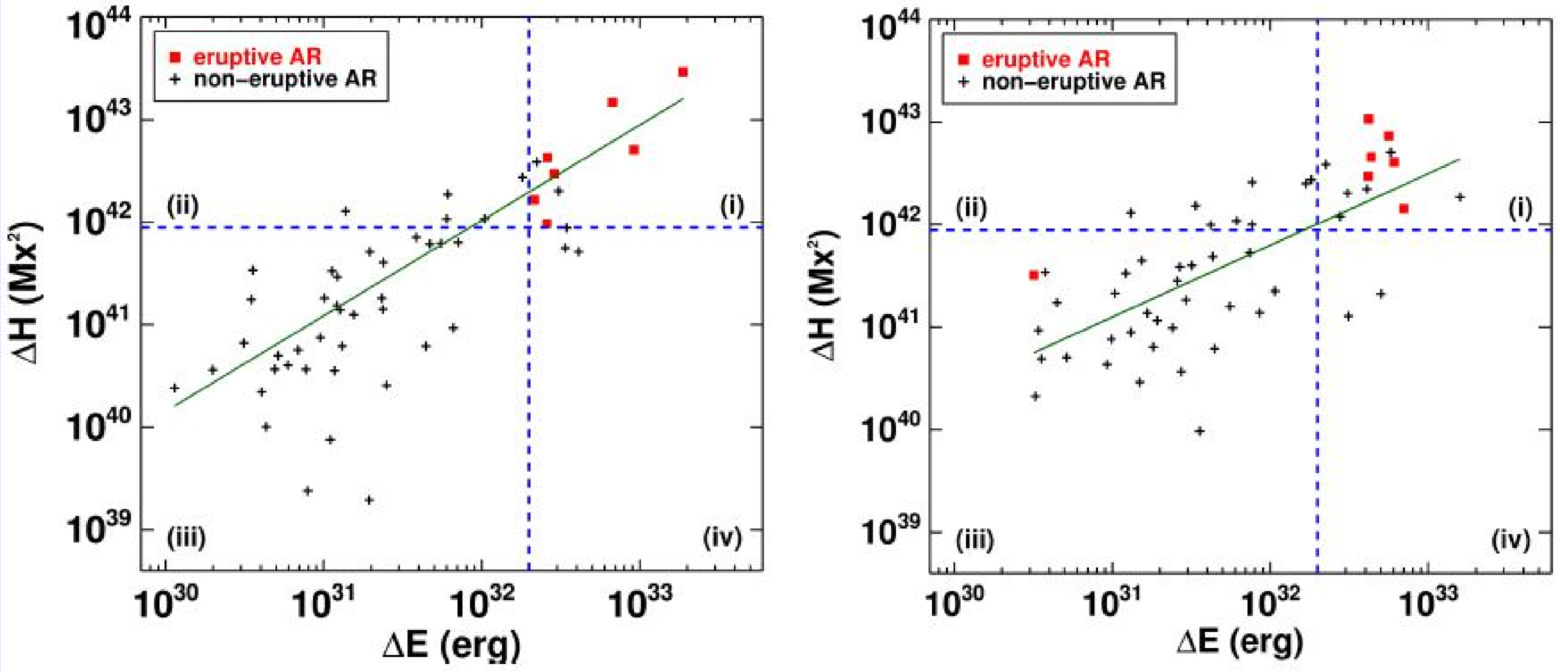


Scatter plots of the accumulated $E_{total}$ vs. absolute $H$ during the flux emergence intervals of ARs (left panel) and during the intervals from emergence start times until the ARs cross W45 or produce their first CME, whichever occurs first (right panel). Red squares and black crosses correspond to eruptive and noneruptive ARs. The blue dashed lines define the thresholds for $H$ and $E_{total}$ above which ARs show a high probability to erupt (Liokati et al. 2022)

-- Thresholds for both the $H_m$ (0.9-2 x $10^{42}$ Mx$^2$) and $E_{free/total}$ (0.4-2 x $10^{32}$ erg) have been established. If these thresholds are exceeded the host AR is likely to erupt (Tziotziou et al. 2012; Liokati et al. 2022)

# Large eruptions may occur at times of helicity and free energy peaks

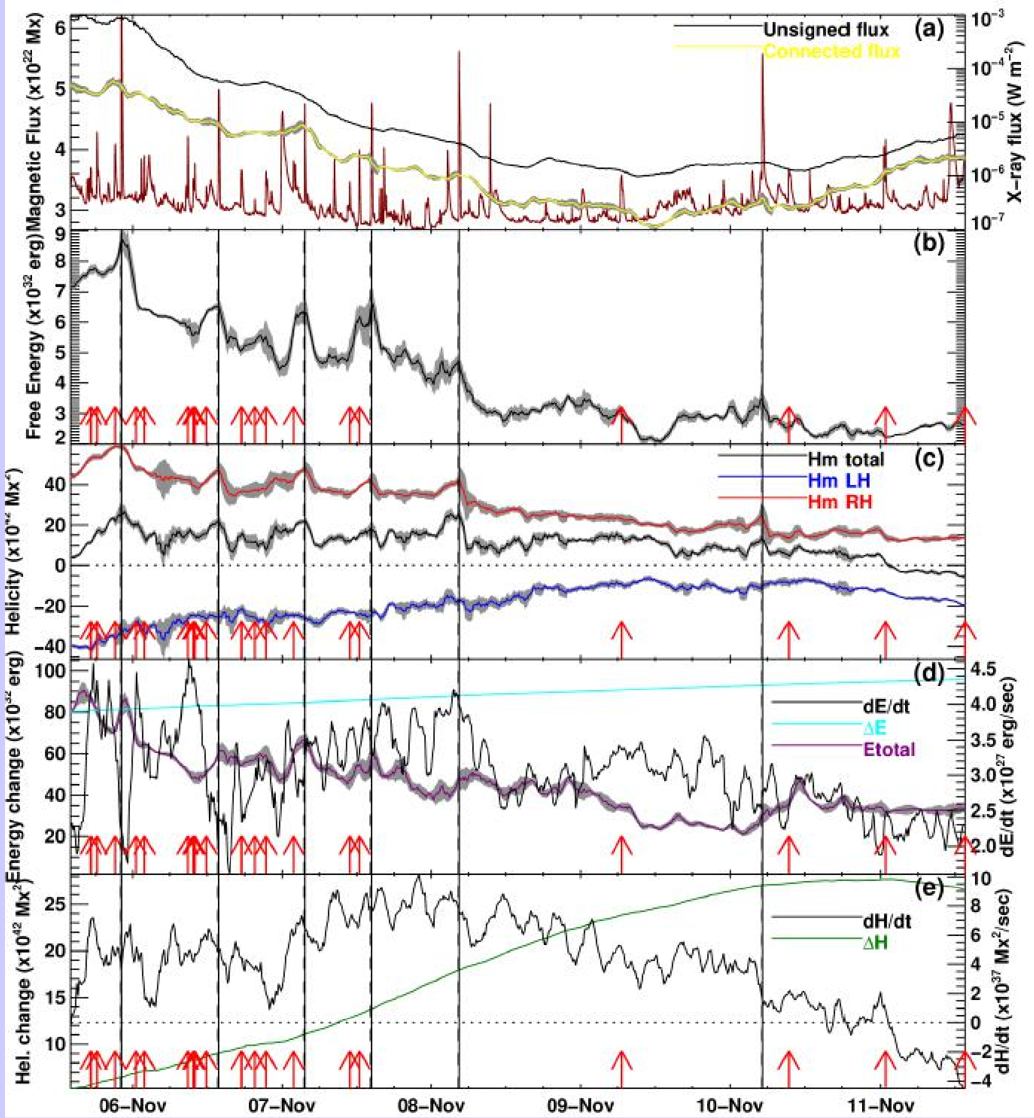


Liokati et al. (2023)

Unsigned magnetic flux
Connected magnetic flux

Free magnetic energy

Net magnetic helicity
Right-handed magnetic helicity
Left-handed magnetic helicity

dE/dt (from FI method)
Accumulated ΔE (from FI method)
Etotal

dH/dt (from FI method)
Accumulated ΔH (from FI method)

- ARs featured substantial budgets of $E_{\mathrm{free}}$ and of both positive and negative $H$
- The imbalance between the signed components of their helicity was as low as in the quiet Sun and their net helicity eventually changed sign 14-19 h after their last major flare
- Despite this incoherence, the eruptions occurred at times of net helicity peaks that were co-temporal with peaks in the $E_{\mathrm{free}}$
- $H$ and $E_{\mathrm{free}}$ losses related to the eruptions ranged from (1.3-20)x$10^{42}$ $Mx^2$ and (0.3-2)x$10^{32}$ erg

# Intensive helicity-related eruptivity proxies

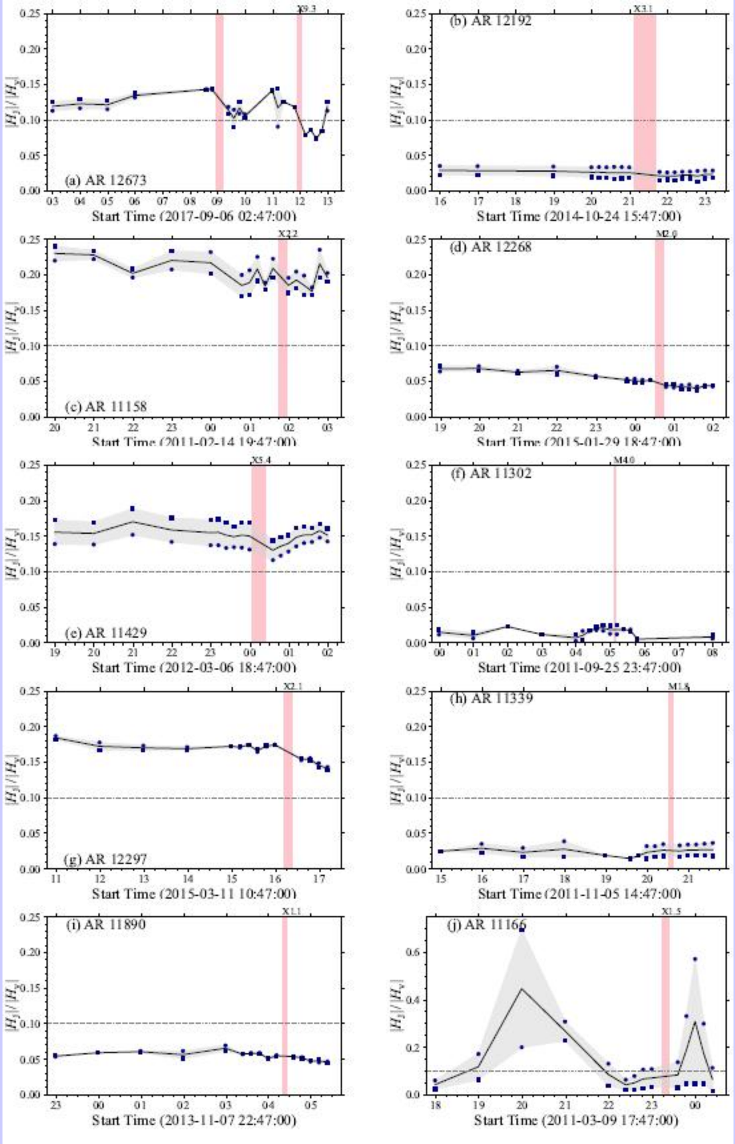

Gupta et al. (2021)

Time evolution of the "helicity ratio", $H_J/H_V$, for 10 ARs. Quantities for ARs productive of large eruptive and confined flares are shown in the left and right columns, respectively. The vertical bar marks the impulsive flare phase

- The total energy and helicity budgets of flare-productive ARs (extensive parameters) cover a broad range of magnitudes, with no obvious relation to the eruptive potential of the individual ARs

- The intensive eruptivity proxies, $E_f/E$ and $|H_J|/|H_V|$, and $|H_J|/\Phi^2$, however, are distinctly different for ARs that produce CME-associated large flares compared to those which produce confined flares

- For the majority of these ARs, Gupta et al. identified characteristic pre-flare magnitudes of the intensive quantities that are clearly associated with subsequent CME-productivity

# Helicity budgets of jets from an emerging active region

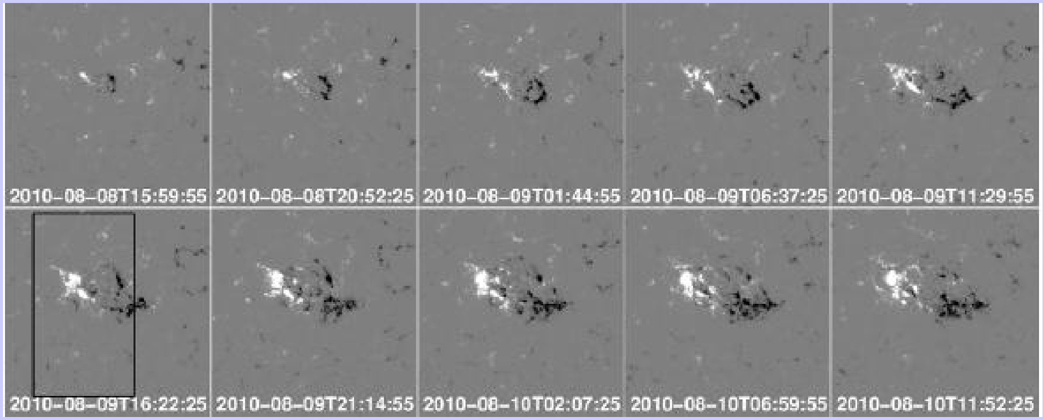


HMI magnetograms

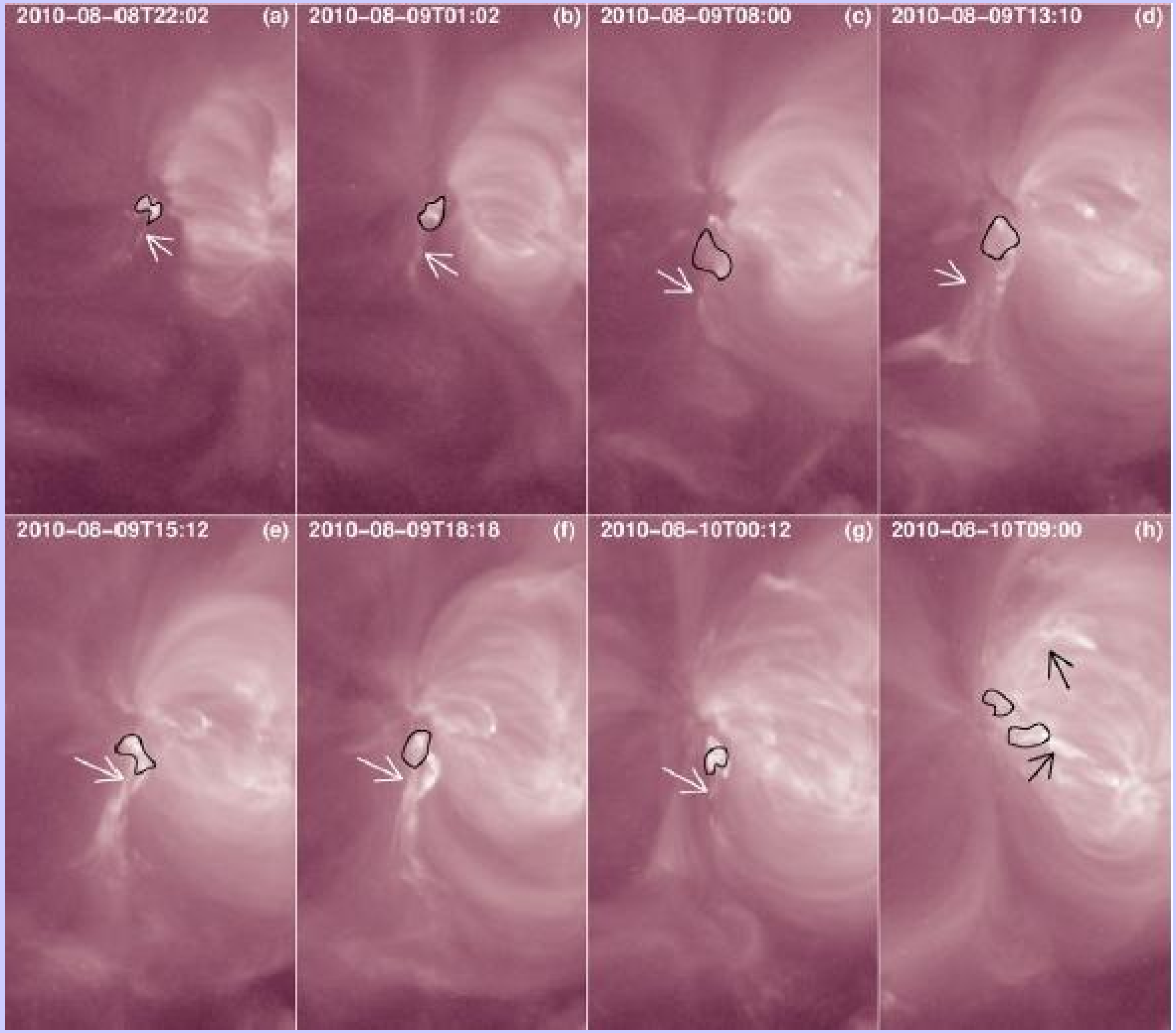


Major jets from the AR

Small bipolar emerging AR that did not produce any CMEs or flares above C1.0, but it was the site of 60 jet events during its flux-emergence phase.

Nindos et al. (2024)

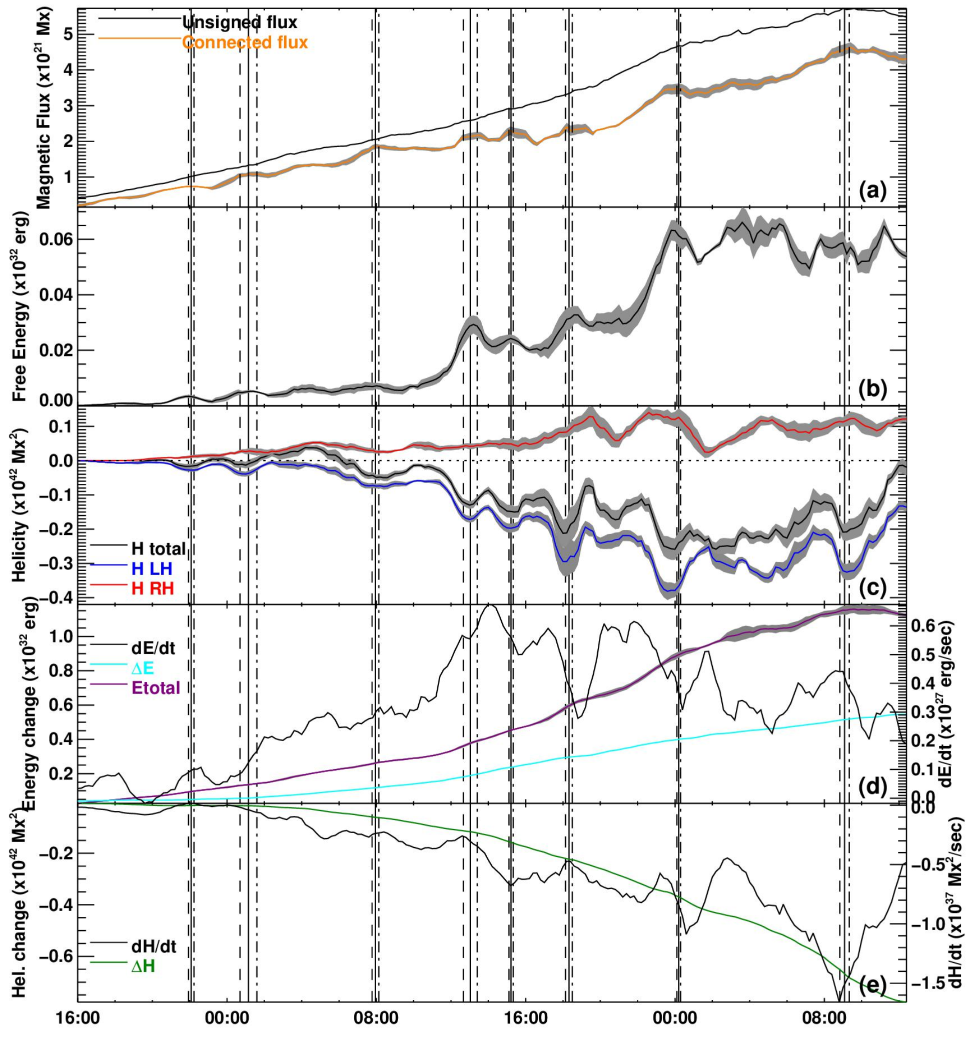


Unsigned magnetic flux
Connected magnetic flux

Free magnetic energy

Net magnetic helicity
Right-handed magnetic helicity
Left-handed magnetic helicity

dE/dt (from FI method)
Accumulated ΔE (from FI method)
Etotal

dH/dt (from FI method)
Accumulated ΔH (from FI method)

- The $H$ and $E_{\mathrm{free}}$ budgets of the AR were below established eruption-related thresholds
- Each of the time profiles of the $H$ and $E_{\mathrm{free}}$ budgets showed discrete localized peaks, with 8 pairs of them occurring at times of jets
- These jets featured larger base areas and longer durations than the other jets of the AR.
- We estimated, for the first time, the $H$ and $E_{\mathrm{free}}$ changes associated with these eight jets, which were in the ranges of 0.5-7.1 x $10^{40}$ $Mx^2$ and 1.1-6.9 x $10^{29}$ erg, respectively.
- Although these values are 1-2 orders of magnitude smaller than those usually associated with CMEs, the relevant percentage changes were significant and ranged from 13% to 76% for the normalized $H$ and from 9% to 57% for the normalized $E_{\mathrm{free}}$.

# Heliospheric connections (I)

HELICITY BUDGETS

| NOAA ACTIVE REGION (1) | $\alpha_{AR}$ [a] (2) | $\Delta H_{LCT}$ ($\times 10^{40}$ Mx$^2$) (3) | $\Delta H_{rot}$ ($\times 10^{40}$ Mx$^2$) (4) | CMEs (5) | $H_{CME}^{tot}$ [b] ($\times 10^{40}$ Mx$^2$) $l = 2$ AU (6) | $l = l_k$ (7) | $l = 0.5$ AU (8) | $(H_{CME}^{tot} - \Delta H_{LCT} - \Delta H_{rot})/H_{CME}^{tot}$ [c] (%) $l = 2$ AU (9) | $l = l_k$ (10) | $l = 0.5$ AU (11) |
|---|---|---|---|---|---|---|---|---|---|---|
| 8210 | + | 3784 | 324 | 9 | 16596 | 9270 | 4149 | 75 | 56 | 1 |
| 8375 | + | 1178 | 334 | 9 | 4428 | 1296 | 1107 | 65 | −17 | −36 |
| 9114, 9115, 9122[d] | − | −1697 | −257 | 3 | −5712 | −2052 | −1428 | 66 | 5 | −37 |
| 9182 | + | 276 | 34 | 4 | 1176 | 404 | 294 | 74 | 23 | −5 |
| 9201 | − | 133 | −428 | 1 | −2980 | −1922 | −745 | 90 | 84 | 60 |
| 9212, 9113, 9118[d] | − | −477 | −666 | 3 | −3582 | −1245 | −895 | 68 | 8 | −28 |

[a] Active region's chirality.
[b] Cols. (6)–(8) refer to the total helicity ejected by the CMEs derived using $l = 2$ AU, eq. (5), and $l = 0.5$ AU, respectively, for the MC helicity computation.
[c] In cols. (9)–(11) the total helicity ejected by the CMEs has been derived using $l = 2$ AU, eq. (5), and $l = 0.5$ AU, respectively, for the MC helicity computation.
[d] The values of $\Delta H_{LCT}$ and $\Delta H_{rot}$ refer to the whole complex of active regions.

Nindos et al. (2003)

- Studied six eruptive ARs that produced halo CMEs which evolved to major geomagnetic storms and magnetic clouds (MCs) at 1 AU.
- Computed accumulated helicity in the ARs using the FI method
- Compared AR helicities with the helicities carried away by the CMEs using the MC helicity computations as proxies to the CME helicities.
- Broadly consistent budgets were derived although discrepancies were not negligible.

# Heliospheric connections (II)

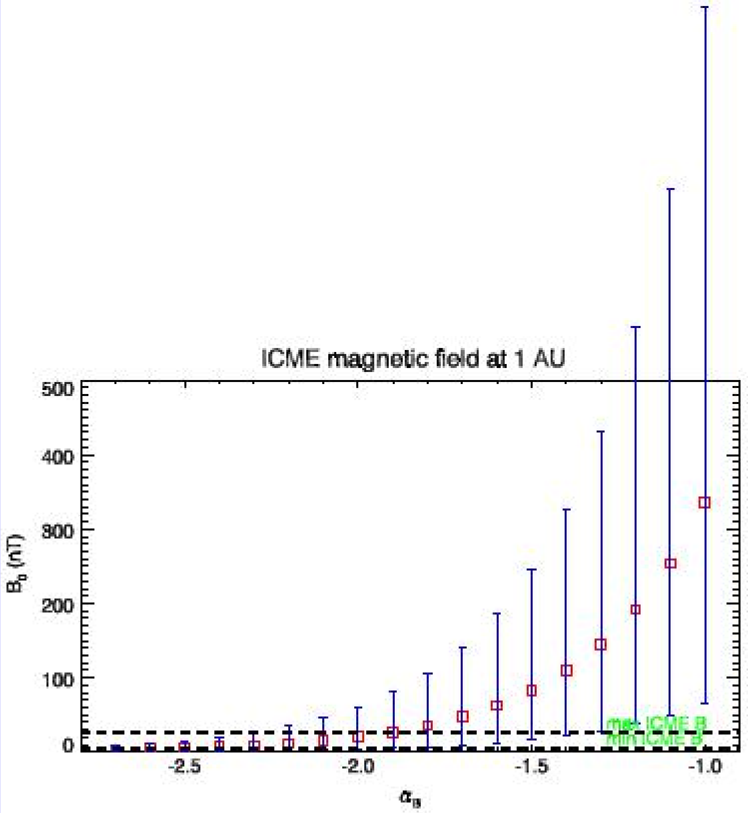


Extrapolated CME magnetic field at 1 AU as a function of the radial power-law index $\alpha_B$ of the magnetic field strength. The squares, lower, and upper error bars correspond to the average, minimum, and maximum values of the CME magnetic field calculated at 13 Rs, respectively. The lower and upper horizontal lines correspond to the minimum and maximum magnetic field magnitude of the associated ICME as deduced from in situ Wind measurements (Patsourakos et al. 2016)

- The magnetic field entrained in a major CME was estimated by means of a method combining helicity calculations in the low solar atmosphere, geometrical modeling in the outer corona (13 Rs) and using helicity conservation and analytical models of flux-rope CMEs

- The resulting magnetic field strengths of the CME were in the range 0.01–0.16 G at 13 Rs (higher by a factor 8–17 than the magnetic fields of the quiescent corona)

- Extrapolations of the inferred magnetic field of the CME to 1 AU require steep ($\alpha_B \approx -2$) radial fall-offs to match the observed magnetic field values of the associated ICME

# Conclusions

- Conserved nature of *H*: useful tool to study several phenomena
- CMEs as valves through which the Sun gets rid of excess helicity
- Helicity thresholds for the production of large eruptive events
- ARs may produce major eruptions even when, in addition to the accumulation of significant $E_{free}$, they accumulate large amounts of both LH and RH helicity without a strong dominance of one handedness over the other
- In most cases, these excess budgets appear as localized peaks, co-temporal with the flare peaks, in the time series of $E_{free}$ and *H*
- Jets may occasionally have a significant imprint in the evolution of helicity and free magnetic energy budgets of emerging ARs
- Reconcile *H* budget from the photosphere to 1 AU
- The conservation of magnetic helicity provides a powerful and elegant method for the calculation of the magnetic field in flux-rope CMEs

# But

- Difficult to compute
- As accuracy of *H* calculations will improve it is possible that new/unexpected phenomena will be revealed
- No info on spatial distribution of helicity
- Concept of “field-line helicity” is promising (see K. Moraitis’ talk)